



OPEN

Metabolic adaptations underpin high productivity rates in relict subsurface water

Betzabe Atencio¹, Eyal Geisler¹, Maxim Rubin-Blum^{2,3}, Edo Bar-Zeev¹, Eilon M. Adar¹, Roi Ram^{1,4,5} & Zeev Ronen¹✉

Groundwater aquifers are ecological hotspots with diverse microbes essential for biogeochemical cycles. Their ecophysiology has seldom been studied on a basin scale. In particular, our knowledge of chemosynthesis in the deep aquifers where temperatures reach 60 °C, is limited. Here, we investigated the diversity, activity, and metabolic potential of microbial communities from nine wells reaching ancient groundwater beneath Israel's Negev Desert, spanning two significant, deep (up to 1.5 km) aquifers, the Judea Group carbonate and Kurnub Group Nubian sandstone that contain fresh to brackish, hypoxic to anoxic water. We estimated chemosynthetic productivity rates ranging from 0.55 ± 0.06 to $0.82 \pm 0.07 \mu\text{g C L}^{-1} \text{d}^{-1}$ (mean \pm SD), suggesting that aquifer productivity may be underestimated. We showed that 60% of MAGs harbored genes for autotrophic pathways, mainly the Calvin–Benson–Bassham cycle and the Wood–Ljungdahl pathway, indicating a substantial chemosynthetic capacity within these microbial communities. We emphasize the potential metabolic versatility in the deep subsurface, enabling efficient carbon and energy use. This study set a precedent for global aquifer exploration, like the Nubian Sandstone Aquifer System in the Arabian and Western Deserts, and reconsiders their role as carbon sinks.

Keywords Ancient groundwater, Carbon fixation, Deep terrestrial subsurface, Metagenomics, Primary production

Deep subsurface terrestrial habitats, including groundwater ecosystems, host ~ 15% of the total biomass in the biosphere¹, comprised mainly of bacteria and archaea, including novel lineages, that play an essential role in biogeochemical cycling^{2,3}. These microorganisms thrive under extreme environmental conditions, such as high temperatures and salinities, by utilizing a variety of energy resources^{4,5}. Although the overall amount of available energy resources is limited, the diversity of these resources—such as hydrogen, methane, and reduced sulfur compounds—allows for microbial adaptation and survival. Yet, the abundance, productivity, and functionality of microbial lineages and their relationship with their environment in these groundwater ecosystems have scarcely been studied.

One of the fundamental questions concerns energy- and carbon-acquisition mechanisms by chemoautotrophic microbes that assimilate inorganic carbon in the dark underground, using multiple metabolic routes and electron donors^{6–8}. These microbes have the potential to thrive in such habitats, including old groundwater, where even trace amounts of microbially produced oxygen can support aerobic metabolism and boost productivity⁹. However, how the heterotrophic secondary producers rework the soluble and particulate organics from the groundwater primary producers is still not fully understood⁷.

Most studies of groundwater microbes and their activity have focused on shallow aquifers, providing extensive insights into microbial community structures, metabolic potential and interactions with geochemical processes^{10–13}. These studies have documented microbial diversity and function in shallow, oxygenated environments, highlighting the role of microbial taxa in nutrient cycling. For example, Overholt et al.¹² found that carbon fixation rates in shallow groundwater (~ 90 m) are similar to those observed in oligotrophic marine systems, underscoring the importance of autotrophic microbes in these environments. In contrast, our knowledge of

¹Department of Environmental Hydrology and Microbiology, Zuckerberg Institute for Water Research, Ben-Gurion University of the Negev, Sede Boqer Campus, Midreshet Ben-Gurion, Israel. ²Department of Marine Biology, Israel Oceanographic and Limnological Research Institute, Haifa, Israel. ³Department of Marine Biology, Leon H. Charney School of Marine Sciences, University of Haifa, Haifa, Israel. ⁴Geological Survey of Israel, Jerusalem, Israel. ⁵Present address: Institute of Environmental Physics, Heidelberg University, 69120 Heidelberg, Germany. ✉email: zeevrone@bgu.ac.il

microbial communities in deep aquifers, especially those with pristine ancient groundwater is limited^{9,14–16}. Few studies such as Pedersen and Ekendahl¹⁴ have shown that microbial communities in deep crystalline bedrock can assimilate CO₂ and introduce organic compounds, indicating active microbial metabolism. Additionally, while there have been studies on primary autotrophic activity in high-temperature environments like hydrothermal vents^{17,18}, similar research is lacking in high-temperature aquifers. These deep aquifers, often characterized not only by high temperature but also brackish waters, present unique ecosystems that are less explored. We addressed this knowledge gap by investigating microbial communities in deep (up to 1500 m below the surface [mbs]), mainly confined aquifers under a hyperarid area with highly pressurized ancient groundwater. We focused on two deep regional aquifers from Israel's Negev Desert—the Kurnub Group Nubian sandstone and the overlying Judea Group carbonate aquifers, hereafter referred to as sandstone and carbonate aquifers.

The initial trigger for this study was the significant biofouling in reverse-osmosis desalination plants processing brackish water from the deep and confined sandstone aquifer (Fig. 1). Despite the aquifer's ancient groundwater, dated via ⁸¹Kr to tens to hundreds of thousands of years^{19–21}, the ages do not monotonically increase downstream as one would anticipate in a confined system. This irregular pattern is also reflected in the fluctuating chemical and isotopic composition along the eastern flow path from the southern Negev toward the outlet at the Dead Sea basin (Fig. 1). A hydrological analysis based on hydrochemistry and isotopic composition suggests groundwater mixing from nearby aquifers, including younger, though still ancient, waters from the carbonate aquifer²². These potentially interconnected aquifers have distinct lithologies, mineralogy, and hydrochemistry^{19,22,23} (see extended review in Supplementary Note 1, Additional File 1), providing an opportunity to study the ecophysiology of microbes in deep, pristine, ancient groundwater. Access to a series of production

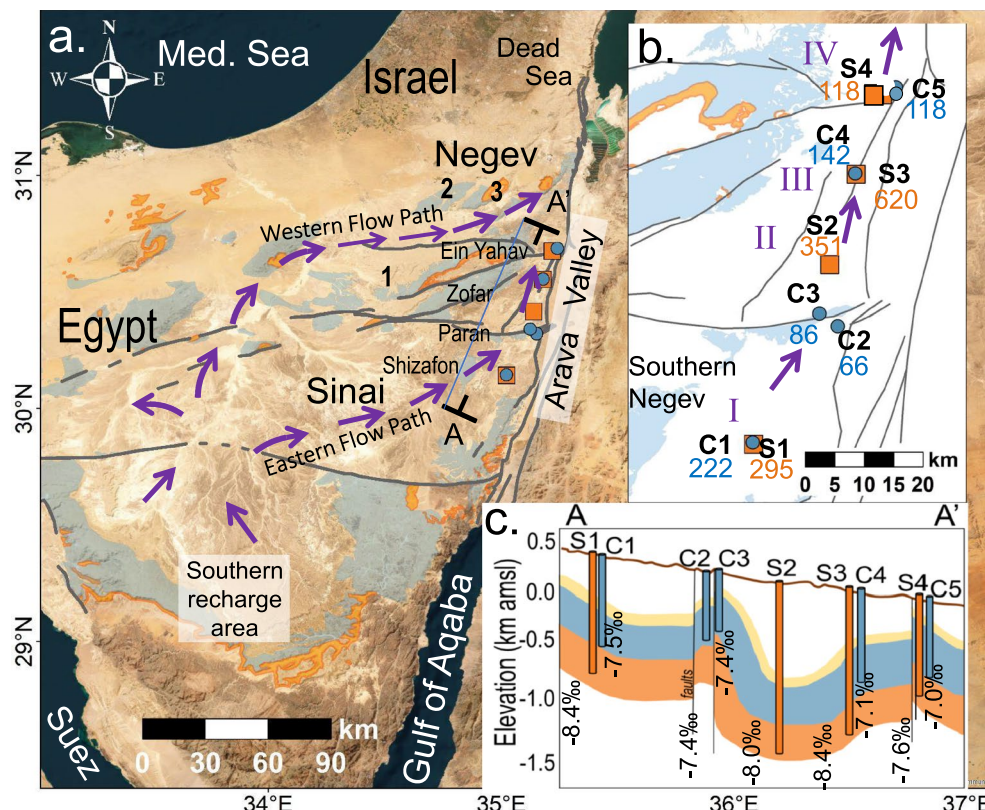


Figure 1. (a and b) Location of wells tapping the sandstone and overlying carbonate aquifers (S and C wells, respectively) along the eastern groundwater flow path (purple arrows) stretching from the southern central Sinai, through the eastern Negev Desert toward the outlet south of the Dead Sea. Also shown are sandstone and carbonate outcrops (orange and light blue shades, respectively) and major geological faults (gray lines) over the Negev Desert. Numbers in panel a indicate some of the major geological anticlines in the studied area: (1) Ramon, (2) Hatira, and (3) Hatzera. ⁸¹Kr ages, reported in thousands of years, are shown in panel b following previous studies^{20–23,25}. The four flow segments discussed in this paper are annotated as I (Shizafon), II (Paran), III (Zofar), and IV (Ein Yahav). (c) A schematic cross-section A-A' along the eastern flow path. Numbers designate $\delta^{18}\text{O}$ values. amsl, above mean sea level. a and b generated with QGIS (<https://www.qgis.org/>). Geographic Information System. Open Source Geospatial Foundation Project (<https://www.osgeo.org/>). Satellite imagery source: Esri, Maxar, GeoEye, Earthstar Geographics, CNES/Airbus DS, USDA, USGS, AeroGRID, IGN, and the GIS User Community. (Satellite imagery source: Esri, Maxar, GeoEye, Earthstar Geographics, CNES/Airbus DS, USDA, USGS, AeroGRID, IGN, and the GIS User Community.)

wells in four segments along the eastern flow path (Fig. 1a), containing fresh to brackish groundwater spanning hypoxic to anoxic conditions, facilitated the investigation of these deep microbial communities.

We hypothesized that (i) the availability of electron donors and acceptors, as well as local conditions such as high temperatures can alter microbial productivity rates and mechanisms of carbon fixation along the eastern groundwater flow path (Fig. 1), (ii) the diversity and function of microbial communities differ between the carbonate and sandstone aquifers, due to differences in formations, hydrogeological features, hydro-physiochemistry and various sources of groundwater recharge.

To address these questions we analyzed long-term hydrogeochemical data from production wells (Fig. 1a), evaluated primary and secondary production (PP and SP), and used metagenomics to study microbial diversity and metabolic potential in interconnected aquifers in the Negev. By employing multifaceted analyses encompassing various data types across multiple sampling sites, we aimed to advance our understanding of microbial communities within deep, pristine aquifers containing ancient water mixed with younger water in certain sections. This study's productivity estimates served to update carbon-sequestration rates in aquifer systems with fossil water.

Methods

Field and laboratory methods

We collected groundwater samples from production wells in the Negev Desert and the Arava rift valley (Fig. 1), as well as from a single, inactive artesian well (S3: Zofar 20) along four selected segments along the eastern groundwater flow path (Fig. 1a,b). To ensure representative groundwater samples, most of the sampled wells were collected from active production wells, which typically do not require purging. We ensured that all these wells were active during the days preceding sampling. An exception is well S3, which is inactive and cased well with artesian groundwater flow. The artesian well (S3) was purged by removing three well volumes before sampling. Physical parameters, such as pH, electrical conductivity (EC), and dissolved oxygen (DO), were monitored throughout the sampling period to ensure representative stable groundwater.

Four samples were collected from the deep sandstone (S wells) and five from the overlying carbonate aquifer (C wells). The screens of the wells are perforated at various depths ranging from 471 to 718 mbs for the carbonate aquifer wells and from 765 to 1478 mbs for the sandstone aquifer wells (Table 1).

Filtered water samples for determination of major ions (SO_4^{2-} , NO_3^- , Ca^{2+} , Mg^{2+} , Na^+ , K^+) were collected in falcon tubes and measured and analyzed by Dionex ion chromatography (ICS 5000) with Chromeleon software (Thermo Fisher Scientific) and employed inductively coupled plasma (ICP) analysis (SPECTRO Analytical Instruments GmbH). HCO_3^- concentrations were determined by automated titration-end point detection using a Metrohm titrprocessor. The analytical methods for $\delta^{13}\text{C}_{\text{DIC}}$ and DIC measurement were as described previously²⁴. Briefly, samples for $\delta^{13}\text{C}$ and DIC analyses were immediately filtered through 0.22- μm filters, stored at 4 °C, and estimated by isotopic ratio mass spectrometry (DeltaV Advantage, Thermo Fisher Scientific). DIC was obtained as a byproduct of the ^{13}C analysis, according to the peak height and a calibration curve. The reported standard deviation was derived from two replicates (Table 1). The measured $\delta^{18}\text{O}$ values are reported

ID	Well name	Depth	Median Screen depth	Field data				Cell abundance	Isotope ratios		$\delta^{13}\text{Kr}$ age ^a	Chemical composition					
				T	DO	EC	pH		$\delta^{18}\text{O}^{\text{a}}$	$\delta^{13}\text{C}_{\text{DIC}}$		NH_4^+	SO_4^{2-}	HS^{b}	TOC	HCO_3^-	DIC
		mbs	mbs	°C	$\mu\text{mol L}^{-1}$	mS cm^{-1}		Cells L^{-1}	%	%	ky	$\mu\text{mol L}^{-1}$	mmol L^{-1}	$\mu\text{mol L}^{-1}$	mmol L^{-1}	mmol L^{-1}	mmol L^{-1}
Carbonate aquifer																	
C1	Shizafon 11	960	666	50	3.1 ^b	3.2	7.32	3.85×10^7	-7.5	n.a	222 ± 20	233 ± 1.7	9.4	4.0	0.08	4.4	n.a
C2	Paran 129	643	580	37	2.8	4.1	6.59	1.33×10^8	-7.4	-2.5	66 ± 12	209 ± 14	14.3	15.2	0.05	5.8	8.9 ± 0.2
C3	Paran 21	963	718	39	4.7	2.8	6.68	6.16×10^7	-7.4	-3.4	91 ± 13	85 ± 2.2	5.8	48.1	0.07	5.6	8.8 ± 0.0
C4	Zofar 220	593	471	41	2.8	2.5	6.87	4.28×10^8	-7.1	-1.4	142 ± 16	261 ± 26	5.3	287	0.07	5.8	7.6 ± 0.2
C5	Ein Yahav 7	710	635	39	4.7	3.2	6.85	1.27×10^7	-7.0	-2.6	118 ± 14	122 ± 13	6.0	74.5	0.09	4.9	5.2 ± 0.2
Sandstone aquifer																	
S1	Shizafon 1	960	854	53	0.9	3.6	6.82	1.16×10^7	-8.4	-3.3	295 ± 16	101 ± 1.07	10.3	9.5	0.08	4.7	$5.0 \pm \text{n.a}$
S2	Paran 20	1536	1415	60	1.3	3.4	6.75	8.72×10^6	-8.0	-4.0	351 ± 14	112 ± 1.9	6.6	25.4	0.08	3.9	4.3 ± 0.5
S3	Zofar 20	1200	920	51	1.3	10	7.16	1.54×10^7	-8.4	-5.9	627 ± 47	146 ± 3.5	8.4	43.4	0.03	2.7	3.5 ± 0.1
S4	Ein Yahav 6	884	822	44	2.2	3.1	7.25	1.88×10^7	-7.6	-5.7	118 ± 14	59 ± 4.2	6.0	92.0	0.08	4.1	5.6 ± 0.2

Table 1. Hydrogeochemical and physical characteristics of the sampled wells in molar concentrations. DO, dissolved oxygen; EC, electrical conductivity; T, temperature; TOC, total organic carbon; DIC, dissolved inorganic carbon; R/Ra, air normalized ratio; ky, thousand of years; mbs, meters below surface; n.a., not available. ^aFrom ^{20–23,25}. ^bFrom the Mekorot National Water Company and the Israeli Water Authority database (unpublished data).

with respect to Vienna Standard Mean Ocean Water (VSMOW) with a standard deviation of 0.1‰ (Table 1); these values were taken from other studies^{20,21,23,25}. Groundwater samples were measured using a Picarro Cavity Ring-Down Spectrometer (L2130-i isotope analyzer) at the Zuckerberg Institute for Water Research Laboratory in Israel. Samples for total organic carbon (TOC) determination were acidified with HCl ($\text{pH} < 2$) and measured in a Sievers InnovOX TOC analyzer (Veolia Water Technologies & Solutions). Ammonia nitrogen ($\text{NH}_4^+ \text{N}$) was determined by the Nessler method²⁶ at 420 nm on a Tecan i-control (Infinite 200). Historical sulfide (H_2S) measurements, based on the standard iodometric method, were obtained from Mekorot National Water Company and the Israeli Water Authority databases.

DNA sampling, extraction, and sequencing

Groundwater samples were collected in clean containers, rinsed in situ with the abstracted groundwater before sampling, and transported immediately to the laboratory facility. Although the filtration process occurred within 12 h after collection. During this time, the samples were kept without any temperature adjustment to maintain their in-situ temperatures and environmental conditions.

Approximately 13 to 50 L of groundwater was filtered using a sterile stainless-steel 142 mm filter holder fitted with a 0.22-µm Durapore filter (Millipore-142 mm; Cat. No. YY3014236, Millipore, Darmstadt, Germany). Samples S1 and C1 were collected in June 2021, and the rest (C2 to C5 and S2, S3, S4) in September 2021. Filters were snap-frozen using liquid nitrogen and stored at -80°C until DNA extraction with the DNeasy Power Water kit (Qiagen) using the manufacturer's protocol.

Library preparation using the NEBNext® Ultra™ IIDNA Library Prep Kit (Cat. No. E7645) and sequencing were performed at the Novogene AIT Genomics facility in Singapore. The nine DNA samples were sequenced using 150 bp paired-end reads on the NovaSeq 6000 platform, with a read depth of ~ 15 Gbp per sample.

Assembly, binning, and metabolic predictions

The DNA reads were assembled with SPAdes V3.14 (-meta, $k = 21,33,66,99,127$)²⁷, following adapter trimming and error correction with tadpole.sh, using the BBtools suite (sourceforge.net/projects/bbmap/). Downstream mapping and binning of MAGs were performed using DASTool, Vamb, Maxbin 2.0, and Metabat2^{28–31} within the Atlas V2.11 framework³², with a genome dereplication nucleotide identity threshold of 0.975. Functional annotation was done with DRAM³³ and METABOLIC³⁴, using default settings and a pathway completeness threshold of 0.75. Key functions were verified using BLAST against NCBI nr/nt and RefSeq databases³⁵. Maximum growth rates were predicted using gRodon2³⁶. DNA raw reads and high-quality MAGs were deposited at NCBI with project accession number NCBI BioProject PRJNA983765.

Primary productivity rates

Groundwater was sampled into sterilized serum bottles (60 mL), overfilled from the bottom, and then crimp-sealed with rubber septa; the samples were kept without any temperature adjustment to maintain their in-situ temperatures. They were transported immediately from the field to an anaerobic hood (Coy Laboratory Products) and transferred into 43 mL glass vials. The ^{14}C -bicarbonate stock solution (aqueous, activity 1 mCi mL $^{-1}$, 17.24 µmol L $^{-1}$, PerkinElmer) was diluted with 3.86 mmol L $^{-1}$ non-radiolabeled bicarbonate. This working solution, with an activity of 5 µCi 50 µL $^{-1}$, was then diluted by a factor of 10^4 once added to the 43 mL sample, representing < 0.0001% of the total DIC in the aquifer samples. The sample's final activity concentration of labeled HCO_3^- was 5 µCi 43 mL $^{-1}$ (1.72 nmol L $^{-1}$ of labeled bicarbonate). The sample was also supplemented with 4.5 µmol L $^{-1}$ of non-radiolabeled sodium bicarbonate. Given that the average bicarbonate concentration across all sites was ~ 4.7 mmol L $^{-1}$, the added tracer's impact on the aquifer's bicarbonate concentrations was negligible. Samples were incubated after spiking with slow rotation for 12 h at in-situ temperature under dark conditions (Benchmark Scientific Roto-Therm Plus, H2024). The incubation temperatures were between 50 to 53 degrees for wells S1 and S3, and between 59 to 60 degrees for well S2, closely matching the in-situ long-term temperatures recorded in the field. At the end of the incubation, all samples were filtered through glass-fiber filters (GF/F, Cytiva, 1,825,025). Hydrochloric acid (50 µL of 37% HCl) was added to the filters overnight to purge the sample of non-assimilated bicarbonate. An additional blank (i.e., no radioactive amendments) was run to evaluate the ambient radioactive background.

The calculation of the added activity is detailed in Supplementary Note 3, Additional File 1. Specifically, 50 µL was taken at the beginning of the incubation ($t = 0$), placed in a GF/F filter, and 50 µL ethanolamine was added to block the purging of radiolabeled bicarbonate from the samples. Radioactively labeled bicarbonate in the collected particulate material was detected as counts per minute by liquid scintillation (Packard Tri-Carb 2100 TR Liquid Scintillation Analyzer). This step was done to estimate the initial radioactive concentration in the samples before incubation, which was obtained by subtracting the initial radioactive concentration of the sample ($t = 0$) from the blank activity. This method was adapted from previous work³⁷ with minor adjustments (see Eq. 1 in Supplementary Note 3, Additional File 1).

Secondary productivity rates

SP rates were estimated by measuring the assimilation rate of radioactively (^{3}H) tagged leucine³⁸. Briefly, sample handling was identical to that for PP measurements. In the anaerobic hood, 1.7 mL groundwater was transferred to a 2-mL HPLC vial $\times 4$ (3 subsamples + 1 blank per well). Leucine (100 µL ^{3}H -Leu, Amersham, specific activity: 160 Ci/mmol, radioactive concentration: 1.0 mCi/mL) was added to the samples, and they were incubated for 12 h in the dark with slow rotation as described above. The incubation was terminated by adding trichloroacetic acid to the samples and storing them at 4°C until measurements were taken (Supplementary Note 3, Additional File 1).

Cell abundance

Subsamples (1.7 mL groundwater) were fixed with glutaraldehyde (Sigma-Aldrich, G7651, final concentration, 0.2%) for 10 min, snap-frozen in liquid nitrogen, and stored at -80 °C until measurements. Samples were thawed at 37 °C, and total cells were stained with SYBR GREEN I (S7563, Invitrogen, final concentration 1 nM, Ex=497 nm, Em=520). We analyzed the samples using an Attune-Next acoustic flow cytometer (Applied Biosystems) equipped with 350 and 450 nm lasers (minor adjustments from³⁹).

Statistical methods and data analyses

All data analyses, including statistics and visualization, were conducted in R version 4.2.3.⁴⁰ Nonparametric Mann-Whitney Test (MWT) was applied to examine the differences in PP, SP, and environmental variables between the aquifers. SigmaPlot 12.5 (Systat Software, Inc.) was also used for data visualization.

Results and discussion

Physicochemical description of water in the sampled wells

Groundwater analyses from the two aquifers showed distinct physical and hydrogeochemical features (Table 1). The median temperatures were 39 °C and 52 °C in the carbonate and deep sandstone aquifers. All samples were hypoxic to anoxic conditions (<0.006 mmol O₂ L⁻¹ or 0.2 mg L⁻¹). EC levels were generally consistent among the samples, with a 3.2 mS cm⁻¹ range. However, sample S3 was exceptional in having elevated salinity levels, with an EC of 10.2 mS cm⁻¹. The redox potential in wells from both aquifers was below -200 mV (unpublished data). Based on water stable isotopes^{20,21,23,25}, the origin of recharge also differed between the aquifers, where the deep Nubian sandstone aquifer presents lower δ¹⁸O values compared to the overlying carbonate aquifer (MWT, *p*=0.020). ⁸¹Kr dating indicates a long residence time of more than 50 thousand years (ky)^{20–23,25}. The sandstone aquifer presents spatial age evolution along the flow path from S1 to S2 (Fig. 1), followed by a sharp increase of more than 200 ky in well S3²⁰. Groundwater in well S3 may represent an intrusion from a deep and older highly pressurized saline aquifer (620 ky, 51 °C), which could have elevated the groundwater age and water temperature in the deep Nubian sandstone aquifer^{20,41}. Further downstream, in well S4, the groundwater age suddenly decreases, which implies younger recharge to these parts of the deep sandstone aquifer²⁰.

Concentrations of potential electron acceptors for microbial metabolism varied across the samples. In the carbonate aquifer, the median 5.6 mmol L⁻¹ bicarbonate (HCO₃⁻) concentration was higher compared to 3.79 mmol L⁻¹ in the deeper Nubian sandstone aquifer (MWT, *p*=0.031). On average, the sulfate (SO₄²⁻) concentrations were 7.76±2.04 mmol L⁻¹ in the sandstone aquifer and 8.34±3.79 mmol L⁻¹ in the overlying aquifer. Nitrate (NO₃⁻) and nitrite (NO₂⁻) concentrations were below detection limits (<0.016 mmol L⁻¹). The electron donors identified in the samples were sulfide (HS⁻) and ammonium (NH₄⁺), whereas methane was not detectable. Sulfide was above 4 μmol L⁻¹ in all wells, with the highest concentration found in C4 from the carbonate aquifer (287 μmol L⁻¹). Ammonium concentration was slightly higher in the carbonate aquifer than in the deep sandstone aquifer (median values of 208 and 107 μmol L⁻¹, respectively). TOC values were below 1 mmol L⁻¹. The isotopic composition of dissolved inorganic carbon (δ¹³C) also varied, reflecting different carbon sources and processes. For example, wells in the carbonate aquifer had δ¹³C ranging from -3.4‰ and -1.4‰. These values may indicate occasional recharge events that dissolve carbonate rocks, enriching the groundwater with higher δ¹³C bicarbonate. Additionally, these recharge events can enhance microbial activity, further influencing the carbon cycle.

High primary productivity rates in the ancient groundwater aquifers

High PP rates were consistently measured (Table 2, Table S1) within the ancient groundwater from two deep wells (S1 and S3) located in the deep sandstone aquifer, characterized by high temperatures (Table 1). By conducting incubations at in situ high temperatures, S3 and S1 exhibited PP rates of 0.545±0.059 to 0.82±0.066 μg L⁻¹ d⁻¹ of fixed carbon (C). Previous research reported carbon fixation rates spanning from 0.043±0.01 to 0.23±0.10 μg C L⁻¹ d⁻¹ within a shallow (90 mbs) carbonate aquifer in Germany with temperatures around 10 °C, and from 0.0095 to 0.0560 μg C L⁻¹ d⁻¹ in the deep (830–1078 mbs) crystalline bedrock of southeastern Sweden with temperatures 21.2–22.9 °C^{12,14,42}. The temperature range of ~ 50–53 °C in our study wells highly differed from the relatively temperate conditions associated with these earlier studies^{12,14,42}. Despite our wells being deep (~ 1000 mbs), the lowest PP rates were marginally overlapping with the highest previously reported rate of 0.23 μg C L⁻¹ d⁻¹ from the 90 m-deep aquifer¹² and almost one order of magnitude higher than in the deep bedrock in Sweden¹⁴. It is suggested that the high PP rates measured herein could be attributed to the unique thermal conditions of our study sites.

ID-Well name	Temperature (°C)	PP± SD (n=3)		SP± SD (n=3)
		μg C L ⁻¹ d ⁻¹	μg C L ⁻¹ d ⁻¹	
S1-Shizafon1	53	0.820±0.066	0.017±0.001	
S2-Paran20*	60	2.14±n.a	0.0173±0.007	
S3-Zofar20	51	0.545±0.0590	0.072±0.001	

Table 2. Primary productivity (PP) and secondary productivity (SP) rates. SD = standard deviation. ° No replicates available. n.a.: not available.

To the best of our knowledge, this is the first report of PP rates in groundwater wells under higher temperature conditions, offering new insights into carbon fixation research. However, it is important to note that microbial activity in hot subsurface environments has been well-documented in other settings, such as hydrothermal vents and deep marine sediments. For example, microbes are active in hydrothermal springs^{17,18}. A significant impact of temperature on carbon fixation has been documented in intertidal sediments and reservoir sediments^{43,44}. Following these findings, we expanded our analysis to include another well (S2), which has a higher temperature (60 °C) compared to wells S1 and S3. This well showed a PP rate of 2.14 µg C L⁻¹ d⁻¹, which is almost an order of magnitude greater than those found in wells S1 and S3, highlighting the potential impact of a temperature increase on PP rates. Owing to the lack of biological replicates for this specific observation, it was not considered as a central element of our analysis. Nonetheless, its integration is essential for a better interpretation of our findings, pointing towards the need for further detailed measurements in subsequent studies. Importantly, the physical, hydrochemical, and isotopic properties of this aquifer system demonstrate a state of pseudo-equilibrium, indicating temporal stability^{20,45,46}. This consistency suggests that the deep, confined aquifer is unaffected by seasonal variations, enhancing the reliability of our PP measurements and providing a consistent view of carbon fixation processes in this unique subsurface environment.

In addition to temperature, other environmental factors likely influence PP rates in aquifers. The distinct rock types and hydraulic properties of the aquifers play crucial roles in the transport and availability of nutrients and electron donors. For instance, sandstone aquifers, as exemplified in our study, are sedimentary rocks that exhibit higher porosity and permeability, thereby facilitating enhanced nutrient flow compared to crystalline rocks such as granite, which are igneous and typically less permeable, as observed in the Swedish study. Moreover, the shallow aquifer in Germany had NH₄⁺ concentrations around 22 µmol L⁻¹⁴², whereas our study reported levels above 100 µmol L⁻¹ (Table 1), indicating higher biological activity likely enhanced by higher temperatures.

Furthermore, local hydrogeological connections between aquifers can introduce additional nutrients and electron donors from adjacent formations. Recent modeling suggests that wells S1 (Shizafon area) and S2 (Paran area) might be hydraulically connected to overlying aquifers, with local fault systems (Fig. 1b) potentially enhancing these connections²². It is likely that the high PP rates could be attributed to both the unique thermal conditions and the availability and transport of nutrients and energy sources.

While our estimates of inorganic carbon fixation in aquifers represent important steps toward understanding microbial carbon cycling in terrestrial subsurfaces, some limitations should be considered. It is important to note that our measurements are based on laboratory measurements that represent the potential productivity and not in situ activity. Furthermore, the conditions in the Negev Desert may not reflect those aquifers from different geological formations and hydrochemical conditions. Future research should aim to address these gaps and minimize the potential biases by incorporating more comprehensive datasets and in situ measurements, ensuring a larger number of sampling points with their replicates to better reflect the heterogeneity of aquifer systems. Our estimates are most applicable to other aquifers that were formerly classified as “fossil,” such as the immense Nubian sandstone aquifers found in the Arabian (Jordan and Saudi Arabia) and the Western (Egypt) Deserts. These regions share similar conditions and may exhibit comparable primary productivity rates.

Linking microbial diversity, its metabolic potential, and productivity

We reconstructed 140 bacterial and 8 archaeal high-quality metagenome-assembled genomes (MAGs) spanning 32 phyla (CheckM 0.94 ± 0.05 completeness and 0.02 ± 0.03 contamination, (Fig. 2, Tables S3-S4). Archaea were usually scarce (0 to 6% read abundance), following previous studies reporting similar patterns in groundwater^{47,48}. The key observed pattern was a predominance of Halothiobacillales 28-57-27 lineage in the overlying carbonate aquifer (Fig. 2). The representative strain in this clade is *Halothiobacillus neapolitanus*, a sulfur-oxidizing chemolithoautotrophic bacterium whose carboxysomes have been studied in detail⁴⁹. The estimated maximum growth rate of Halothiobacillales MAGs at < 5 h exceeded those of most other autotrophs (e.g., Burkholderiales MAG325—8.2 h, Ammonifexales MAG163—11.6 h, Thermodesulfobacteriales MAG42—10.7 h, Fig. 2). Thus, Halothiobacillales are likely contributors to chemosynthesis in groundwater from the carbonate aquifer.

The southern-most Shizafon site (Fig. 1, wells S1 and C1 abstracting groundwater from the sandstone and carbonate aquifers, respectively) stood out as the sulfur-oxidizing Rhodocyclaceae UBA2250 sp004323595 lineage (Burkholderiales, corresponding to the GCA_004323595.1 NCBI submission previously identified as *Sulfuricystis*⁵⁰) was predominant in both carbonate and sandstone aquifers. In well S1, the ammonia-oxidizing *Nitrosotenius* and Nitrospiraceae (MAG28 and MAG149, 5.8 and 2.6% read abundance) were common, indicating that nitrification can also contribute to carbon fixation. For instance, “*Candidatus Nitrosotenius aquarius*” has been shown to play a significant role in carbon fixation through nitrification in biofilters⁵¹. Similarly, Nitrospiraceae, known for their nitrite-oxidizing capabilities, further facilitate this process by converting nitrite to nitrate, supporting a continuous nitrogen cycle that fuels autotrophic carbon fixation⁵².

Other boreholes extracting groundwater from the sandstone aquifer (S2, S3 and S4) were mainly inhabited by Ammonifexales, Thermodesulfobacteriales, Rhizobiales, Desulfotomaculales, and other rare communities (see alpha and beta diversity analyses in Supplementary Fig. S3, Additional File 3). Interestingly, the deepest sandstone well, S2, also harbored a portion of the dominant community found in the overlying carbonate aquifer (Halothiobacillales 28-57-27), despite possessing distinct hydrochemical properties and significantly higher temperatures compared to the more temperate carbonate wells.

Metagenomics analysis suggests that the potential to fix carbon is widespread among the aquifer taxa (Figs. 2, 3a and Supplementary Table S5-S6, Additional File 2). Among the 140 MAGs reconstructed, 60% of them carried genes indicative of autotrophic carbon fixation capabilities. The key pathways included the Calvin–Benson–Bassham (CBB) cycle, the reductive Krebs (rTCA) cycle, the autotrophic 3-hydroxypropionate/4-hydroxybutyrate (3-HP/4-HB, only in ammonia-oxidizing archaea, 3 MAGs) cycle, and the Wood–Ljungdahl (WL)

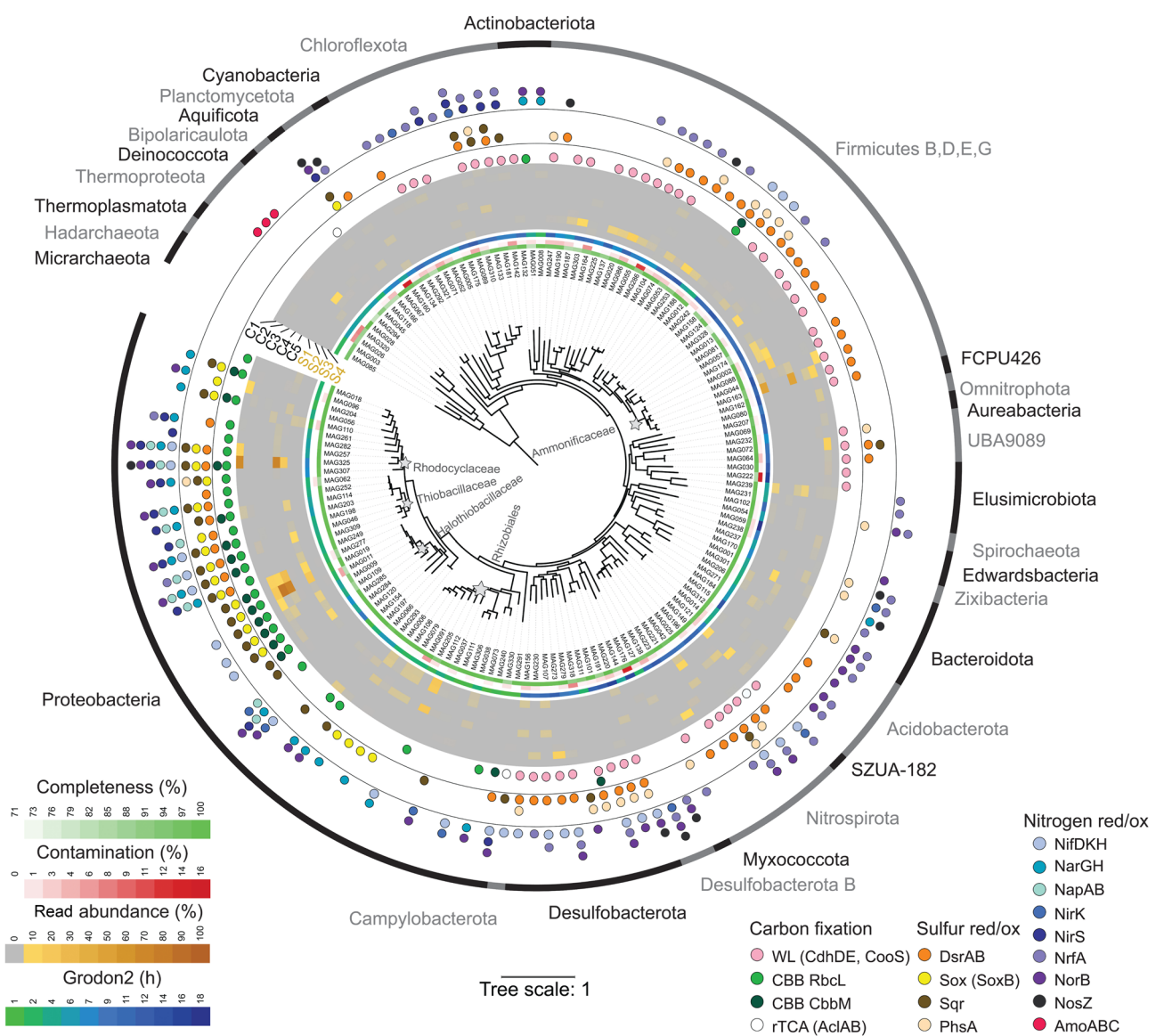


Figure 2. The phylogeny, diversity, and key functions of bacteria and archaea in sandstone and carbonate aquifers. The iTOL representation is based on the GTDB-tk marker gene set and treeing. Key metabolic pathways are indicated in different colors. A heat map shows the median read coverage of each metagenome-assembled genome (MAG) per sample site. MAGs representing the key lineages at the family level are highlighted in bold. Three MAGs were excluded from the tree due to insufficient marker gene hits (27—Riflibacteria, 189—Desulfotomaculaceae, and 217—Rhizobiales). Estimated growth rates for key lineages were calculated based on the Gordon 2 method in hours (h).

pathway (Figs. 2, 3a). In most wells, CBB was the key pathway to fix carbon (Fig. 3a). Ribulose-1,5-bisphosphate carboxylase/oxygenase (RuBisCO) was encoded by 32 MAGs (16 encoded form I, 2 form II, and 14 both forms) (Fig. 2). Both forms were encoded by the most abundant MAGs, representing the populations of Halothiobacillaceae (MAGs 9, 11, 19, 109, 277 and 285), Rhodocyclaceae UBA2250 sp004323595 (MAG325), and *Thiobacillus* (MAG114). These RuBisCO forms differ in their affinity to oxygen and inorganic carbon, as form I enzymes in Halothiobacillaceae function better under high O₂ and low CO₂ conditions, and the opposite holds for form II^{53,54}. Thus, these key autotrophs may be adapted to fluctuating concentrations of oxygen and CO₂. Additional adaptations include maintaining various forms of cytochrome oxidase (for example, the key Halothiobacillaceae MAG019 encoded both the b(o/a)₃-type and the high-affinity cbb3-type terminal cytochrome oxidases). In turn, Rhodocyclaceae MAG325 encoded only the cbb3-type cytochrome oxidase and carried a complete set of genes needed for the denitrification of nitrate to dinitrogen (Fig. 2), suggesting facultative dependence on oxygen.

A limited number of MAGs encoded the rTCA, in particular, the AclAB subunits of ATP-citrate lyase (Nitrosopiraceae MAG149 and *Sulfuricurvum* MAG291, but also the less studied taxa, such as *Bipolariaulota* MAG166 and *Ozemobacteraceae* MAG27). Among these lineages, *Sulfuricurvum* was abundant in carbonate aquifer well C5 (circa 10% read abundance), where DIC was lowest, and there was a notable influence of younger recharge events (Table 1).

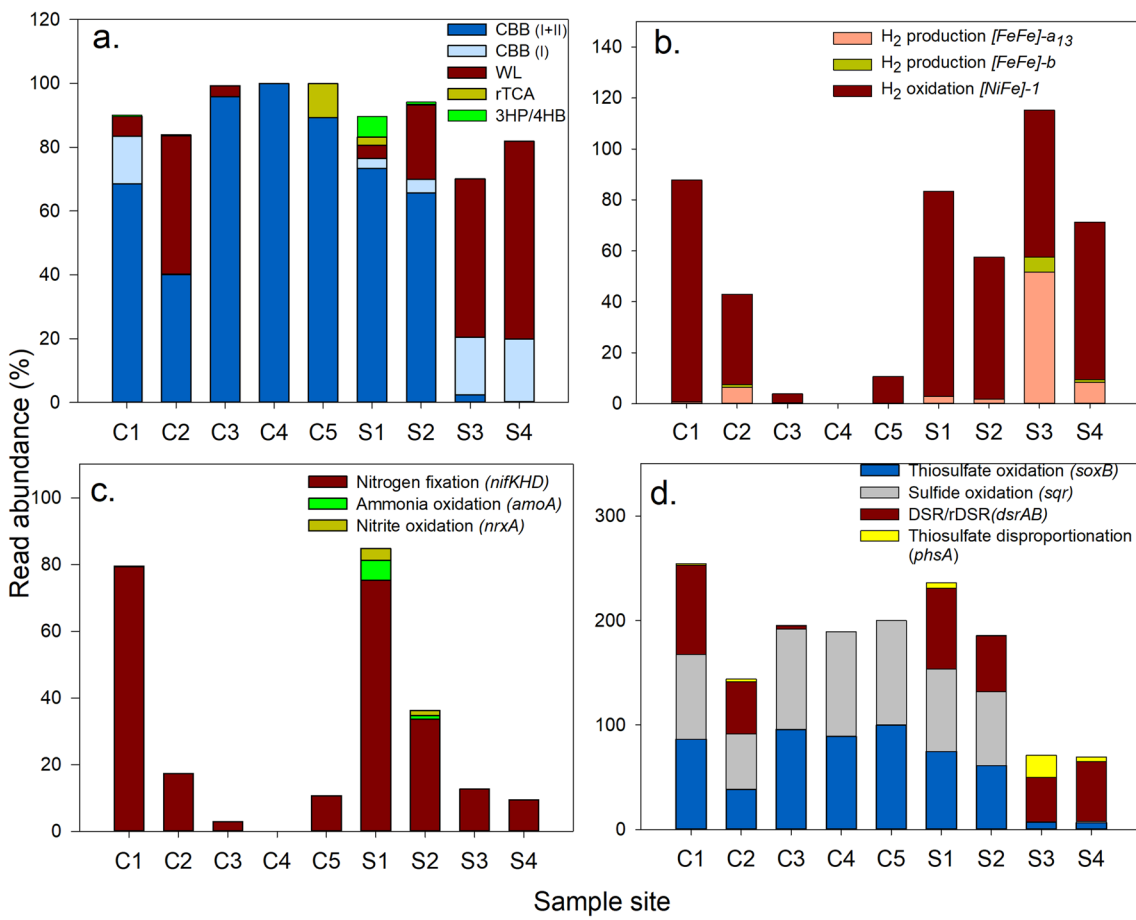


Figure 3. Key metabolic features of microbes in the carbonate aquifer (wells C1 to C5) and sandstone aquifer (wells S1-S4). The cumulative read abundance of metagenome-assembled genomes (MAGs) that encode: **a** carbon fixation; **b** hydrogenases; **c** nitrogen fixation and nitrification; **d** dissimilatory sulfur cycling. CBB—Calvin–Benson–Basham cycle; rTCA—reductive Krebs cycle; WL—Wood–Ljungdahl pathway; DSR/rDSR—dissimilatory sulfur metabolism. The stacked bar chart format presents the percentage of reads mapped to MAGs with these specific genes or pathways, showing the relative abundance of each metabolic feature in the aquifer samples.

The abundance of microbes encoding the energy-demanding CBB cycle was present in all wells of the carbonate aquifer but specifically decreased in well C2 (Fig. 3a). In the sandstone aquifer, the CBB cycle abundance remained similar in wells S1 and S2 but decreased in wells S3 and S4, following the downstream flow direction (Fig. 3a). In S3 and S4 wells, microbial communities appear to employ the WL pathway. We found all three essential genes of the WL pathway (*cdhD*, *cdhE*, and *cooS*) in 50 MAGs (Figs. 2, 3a and Supplementary Fig. S4, Additional File 3). Most of these phyla comprise the anaerobic sulfate reducers and acetogens abundant in the sandstone aquifer and one well from the carbonate aquifer (C2). However, sulfate reducers and other acetoclastic microbes use this route not only to fix CO₂ but also for energy conservation⁵⁵. Thus, we could not rule out that some organisms coding for this pathway may not be fixing carbon⁵⁶.

In the wells where PP was measured, specifically wells S1 and S3, a significant portion of their MAGs demonstrated capabilities for carbon fixation. Specifically, 55% of the total MAGs in well S3 and 68% in well S1 were associated with autotrophic carbon fixation. Notable among these were MAG188 *Desulfotomaculum* in S3 and MAG325 Rhodocyclaceae in S1, representing abundant taxa within their respective wells. This data highlights the PP measurements in these locations and the genetic potential for carbon fixation present within these MAGs.

Our study also revealed insights about the varying presence of autotrophic carbon fixation pathways in fresh to brackish groundwater under hypoxic to anoxic conditions. In the S3 well, characterized by high salinity and the oldest groundwater age estimated at 620 ± 47 ky^{20,25}, the expected dominance of the WL pathway was supported by our observations. This autotrophic pathway is favored by autotrophs under salt stress conditions for its energy efficiency⁵⁶. It also requires anoxic conditions due to the oxygen sensitivity of critical enzymes like acetyl-CoA synthase⁵⁴. Moreover, this autotrophic pathway has been noted as a significant contributor to primary production in deep terrestrial environments^{15,16}.

In contrast, the CBB cycle was the dominant autotrophic pathway in the other wells, S1 and S2 (sandstone), and C1, C3, C4, and C5 (carbonate). The dominance of the CBB cycle, particularly in wells C1, C3 to C5, could be attributed not only to salinity levels but also to occasional recharge events in this carbonate aquifer through the more extensive outcrops⁵⁷ as evidenced by higher $\delta^{18}\text{O}$ (Table 1) compared to the deeper sandstone aquifer. This

might lead to less frequent MAGs with the WL pathway, possibly due to oxygen introduction during recharge, making the WL pathway less favorable despite reports of hypoxic to anoxic conditions across all wells.

Nevertheless, our findings align with previous research that reports the occurrence of both the WL and CBB pathways in groundwater environments across various depths and salinities^{8,58,59}. Our findings indicate a diversity of carbon fixation pathways in groundwater environments, influenced by factors such as anoxia, salinity levels, temperature, groundwater confinement, and isolation. This study provides a foundation for understanding these processes, with future integration of metatranscriptomics potentially offering deeper insights.

Dissimilatory sulfur, hydrogen, and nitrogen metabolism fuels aquifer productivity.

The results suggest a wealth of reducing substrates and electron acceptors for chemosynthesis. Our data indicates an array of sulfur, hydrogen, and nitrogen transformations in the studied aquifers (see Supplementary Tables S7–S11, Additional File 2, Supplementary Fig. S5–S6, Additional File 3). We observed a broad range of sulfide (H_2S) levels (4 to 287 $\mu\text{mol L}^{-1}$) and high concentrations of ammonium (NH_4^+) (up to 233 $\mu\text{mol L}^{-1}$) (Table 1).

While we did not measure dihydrogen concentrations in the Negev groundwater, the common occurrence of hydrogenases described below points to the potential role of hydrogen cycling for microbial productivity (Fig. 3b). Nitrification is another putative driver of carbon fixation in these aquifers (see Supplementary Table S10, Additional File 2). In particular, wells S1 and S2 (sandstone) and C1 (carbonate) showed the presence of bacterial and archaeal ammonia oxidizers and high NH_4^+ levels (Fig. 3c). The archaeal Thermoproteota MAGs carried the *amoABC* operon, encoding the ammonia monooxygenase needed to fuel its carbon fixation (Figs. 2 and 3c). Of 6 MAGs encoding nitrite oxidation to nitrate (*nrxA*), 2 could fix carbon via the rTCA and WL pathways (Nitrospiralia MAG149 and Thermodesulfobacteriia MAG25). Given that nitrite concentrations were below detection limits across all samples (< 0.016 mmol L^{-1}), the cryptic turnover of nitrogen oxides (NOx) is likely. These observations suggest nitrification can fuel primary productivity, even in hypoxic to anoxic aquifers.

We identified 22 MAGs encoding the Sox Kelly–Friedrich pathway for thiosulfate/sulfide oxidation in both sandstone and carbonate aquifers (mostly the chemosynthetic taxa Halothiobacillales, Burkholderiales, Rhizobiales and Campylobacterales, Figs. 2 and 3d). Specifically, the key Halothiobacillales MAG19, Rhodocyclaceae UBA2250 MAG325, and other MAGs like *Thiomonas* MAG056, and *Schlegelella* MAG204 were found to encode the Sox system (genes *soxA*, B, C, D, X, Y, and Z), suggesting that their energy conservation is based on sulfur compounds other than sulfide, such as thiosulfate (Fig. 2).

Sulfate reduction is likely the prevailing anaerobic respiration pathway in both aquifers, following the high sulfate and sulfide concentrations (Table 1). We identified 58 MAGs containing dissimilatory sulfate reduction (DSR) and reverse (r) DSR (encoded by the *dsrAB*) metabolism, including the Rhodocyclaceae UBA2250 MAG325 from Shizafon wells. (Figs. 2,4,3d). We also identified additional *dsr* genes, some of which are specifically associated with sulfur-oxidizing bacteria (such as *dsrEFH*) and others with sulfate-reducing bacteria (e.g., *dsrD*)^{60,61}. The delta subunit of dissimilatory sulfite reductase (*dsrD*) was identified at all sites, except in sites C4 and C5 where it was absent. MAGs containing this subunit were associated with the QYQD01, Desulfotomaculales, Thermodesulfobacteriales, Ammonifexales, and Desulfobacterales orders. In contrast, *dsrEFH* genes were mainly found in MAGs from the Burkholderiales order, specifically within the UBA2250 genus, *Thiobacillus*, *Sulfuritortus*, and an unclassified group PFJX01 within the Thiobacillaceae family. These MAGs showed high abundances in sites C1, S1, and S2, with respective percentages of 80, 75, and 29%. Some key lineages carried the thiosulfate reductase/polysulfide reductase (the *pshA* gene) and thus can disproportionate thiosulfate, yielding sulfate and sulfide (Figs. 3d, 4 and Supplementary Table S7, Additional File 2).

Following previous studies in groundwater^{8,62}, our results highlight the potential use of hydrogen as an energy source, potentially driving carbon fixation. Among the 58 MAGs containing *dsrAB*, we identified 43 MAGs encoding group 1 [NiFe] hydrogen-uptake hydrogenase (Fig. 3b and Supplementary Table S8, Additional File 2), which can couple hydrogen oxidation to sulfate respiration. Furthermore, 23 of these 43 MAGs encoded the WL pathway. For instance, Nitrospirota MAG42, Firmicutes MAG74, and Desulfobacterota MAG220 contained the *hndB* genes (EC 1.12.1.3) predicted to be involved in anaerobic hydrogen oxidation coupled with sulfate reduction, thereby potentially producing energy and fixing carbon via the WL pathway (see Supplementary Table S9, Additional File 2). In addition, we observed the presence of [FeFe] hydrogenases, which are typically linked to the production of H_2 during fermentation (Fig. 3c)⁹. This was evident in Firmicutes MAGs 13, 20, and 303, common in well S3. Most importantly, multiple [Ni–Fe] hydrogenases (uptake—group 1, group 2bc; bidirectional—group 3abd) were found in Shizafon producers Rhodocyclaceae UBA2250 MAG325.

Hydrological investigations have reported the presence of radioactive elements such as radium, radon, and uranium in the Rift Valley's groundwater, which includes water from the Arava Valley^{63,64}. This indicates potential water radiolysis, a process that occurs during radioactive elements' decay and can produce hydrogen, which microbes can utilize as an energy source⁶⁵. The significance of this process is important also by the recent findings of hydrological connections between the sandstone and adjacent aquifers, potentially facilitating the movement of hydrogen across these systems²². Thus, the potential generation of hydrogen in the Arava's groundwater, including our study area, and the presence of various hydrogenases suggest that hydrogen may fuel microbial activity in the Negev and Arava Desert aquifers, particularly the deeper sandstone aquifer; nevertheless, concentrations and sources of hydrogen remain to be determined.

In oxygen-limited aquifers, denitrification could play an essential role in microbial energy conservation⁶⁶. Nitrate reduction to nitrite was encoded by 24 MAGs, including those of the prominent Rhodocyclaceae (Burkholderiales) (Fig. 2, Supplementary Table S11, Additional File 2, and Supplementary Fig. S5, Additional File 3). We could trace complete denitrification to N_2 , mainly by gammaproteobacterial lineages, including the dominant Rhodocyclaceae UBA2250 MAG325, which encoded the periplasmic nitrate reductase (Nap), nitrite reductases NirBD and NirS, nitric oxide reductase NorBC, and nitrous oxide reductase NosZ. However, most microbes

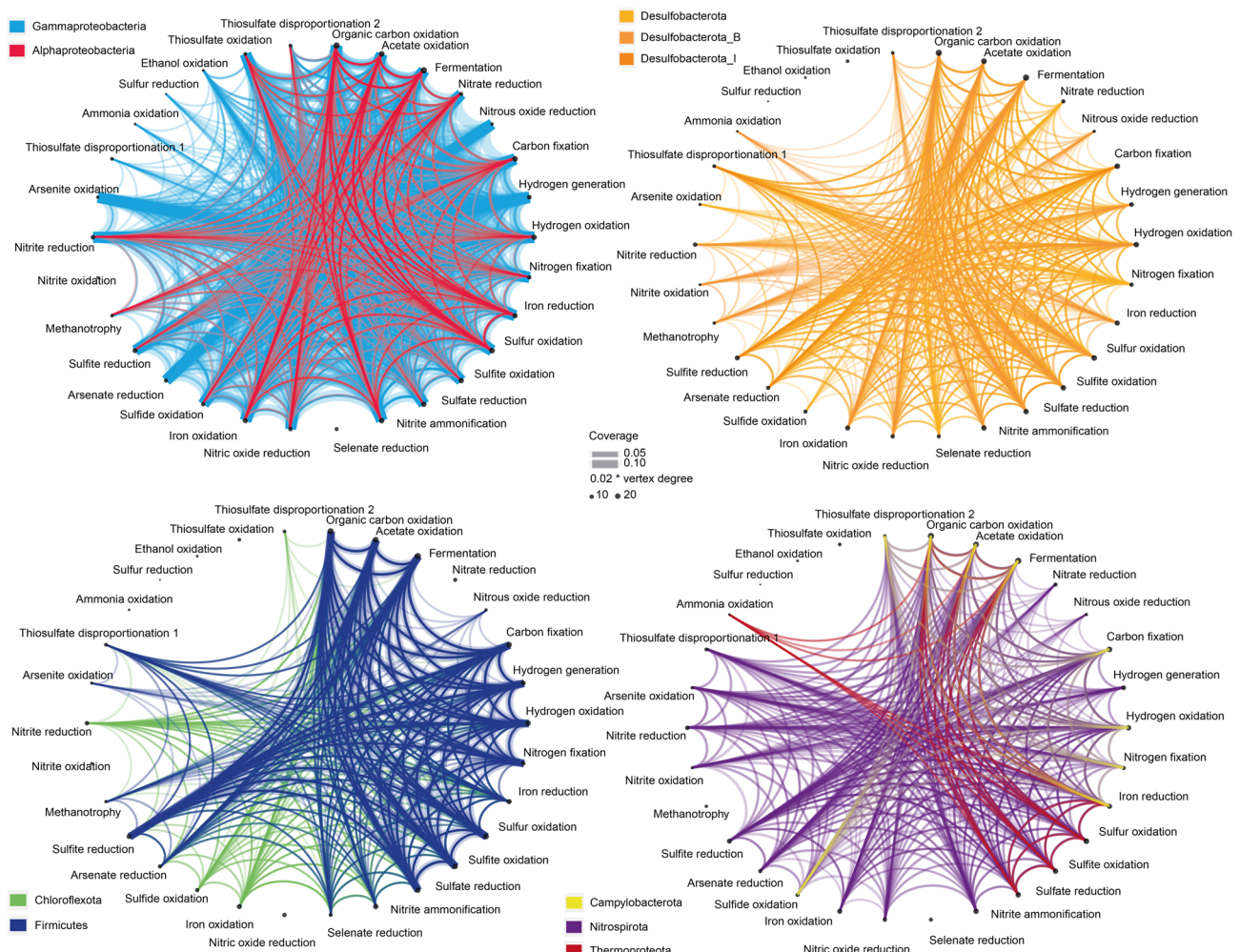


Figure 4. Taxonomic affiliation of metabolic functions in the aquifer community. Key lineages are highlighted in colors. Vertex sizes correspond to the number of connections. Taxa are presented at the phylum level (only Gammaproteobacteria and Alphaproteobacteria are at the class level to display the marked differences within the Proteobacteria).

could only complete parts of the entire route; for example, most Thiobacillaceae encoded all steps except for the final reduction of N_2O to N_2 , whereas some anaerobes encoded only the last step. Overall, 21 MAGs encoded nitrate respiration via the respiratory nitrate reductase NarGHJI, 40 encoded NirBD, 9 NirK, 18 NirS, 34 NorB (18 NorC) and 11 NosZ. This indicates that aquifer communities can denitrify, either egoistically (mainly in wells S1, S2, and C1) or synergistically (see Supplementary Fig. S5, Additional File 3).

The dissimilatory nitrate reduction to ammonia (DNRA) can also contribute to overall productivity under hypoxic conditions, as observed in a karst aquifer⁶⁷. In support of this assumption, we identified 44 MAGs encoding the NrfA nitrite reductase often used in DNRA, especially prominent among anaerobes such as Chloroflexota and Acidobacteriota (Fig. 2). Our findings agree with previous studies that reported the importance of the nitrogen cycle in groundwater with low levels of inorganic nitrogen^{66,68}.

Although no direct measurements of denitrification activity were conducted in our study, the identification of these genes provides an initial indication of potential denitrification processes in these aquifers. Future research, including direct assessments of denitrification and nitrification activities, would be valuable to further elucidate these processes in groundwater ecosystems.

Genomic evidence for nitrogen fixation in pristine groundwater

We identified 26 MAGs encoding the key proteins of the nitrogenase complex (*nifD*, *nifK*, and *nifH*) within diverse taxa, including the anaerobic sulfate reducers Desulfobacterota, Firmicutes (Desulfotomaculia) and Nitrospirota (Thermodesulfobacteriota), the poorly studied lineages such as SZUA-182, and the prominent chemosynthetic lineages, including the common Rhodocyclaceae and Thiobacillaceae (including the abundant UBA2250 MAG325), various Halothiobacillaceae, Sulfurimonadaceae and Nevskiaeae (Figs. 2, 3c and Supplementary Table S10, Additional File 2). The high energy demand of nitrogen fixation may be met under the aquifer's low dissolved oxygen levels by sulfur oxidation and reduction dynamics, using trace oxygen or nitrate as

an electron acceptor. However, the high ammonium concentrations (Table 1) indicate that nitrogen may not be a limiting nutrient in the pristine groundwater unless micro-niches where nitrogen is limited exist (e.g., around mineral grains or organic matter). It has been hypothesized that fixed nitrogen supports subsurface biomass⁶⁹, but nitrogen budgets and rates of N₂ fixation in these systems remain to be elucidated.

What are the sources of compounds that drive productivity in Negev wells?

The sources of key compounds that drive productivity, such as oxygen, nitrate, sulfide, ammonium, and methanol, are not fully understood. We note that oxidation of organics, fermentation, and acetate oxidation are the most characteristic traits of the aquifer microbiome (Fig. 4). Alongside the specialist producers, we find a diverse heterotrophic/mixotrophic community that benefit from reworking the necromass and exudates of the primary producers. The turnover of microbial biomass (necromass) by fermenters is a likely partial source of hydrogen and ammonia, which, as described above, can fuel productivity. These organisms drive SP that is lower than PP (SP/PP = 0.02–0.13; see Supplementary Note 2, Additional File 1, Supplementary Table S2, Additional File 2). The results may reflect the slow heterotrophic metabolism in a hypoxic to anoxic environment. We note that similar proportions of PP and SP were observed in chemosynthetic mats associated with gas seeps in the deep sea⁷⁰ (and in the polar oceans⁷¹.

One factor that might explain the low SP rates is the measurement method. SP was measured solely through leucine assimilation, which may underestimate SP rates by not accounting for organic carbon uptake from in situ substrates. However, while this method may underestimate SP rates, it remains a widely accepted approach due to its specificity for bacterial protein synthesis and carbon production.

Another consideration is the dense mineral matrix characteristic of the aquifers. This dense matrix may restrict the flow and accessibility of fixed carbon to secondary producers. Thus, properties such as permeability and porosity of the aquifer are crucial factors that influence subsurface water movement and the availability of organic molecules for microbial activity. As groundwater percolates through these aquifer layers, the organic carbon undergoes attenuation processes such as molecular filtration⁷². In some cases, the pore sizes within these aquifers are even smaller than the organic molecules⁷², reducing their availability for microbial secondary producers.

In our study, the sandstone aquifer within the Lower Kurnub formation is characterized by fine-grained sediments with small (0.02 µm) pore throats⁷³. The narrow passages between the pores in the Nubian sandstone formations, which contain a carbonate cement with traces of clay mineral, might enhance the electrokinetic attenuation by the electrostatic double layer and, consequently, might lead to a further narrowing of the effective passage through which molecules can move⁷⁴. Studies by Nativ et al.⁷⁵ and Calvo and Gvirtzman⁷⁶ reported core-scale porosity values up to 15% and permeability values up to 2000 md (millidarcys). Hydraulic conductivity values range from 10⁻³ to 10⁻² cm/s, corresponding to a permeability of 1000 md⁷⁶. These values indicate a moderate potential for water movement. However, the small pore sizes and specific mineralogical and lithological composition still can hinder the movement of larger molecules, including dissolved organic molecules.

In addition, the aquifer's age can influence organic carbon availability. It has been reported that older aquifers contain up to 41% less organic carbon than younger ones⁷². Furthermore, it has been suggested that old dissolved organic matter, such as that found in deep groundwater is considered recalcitrant⁷⁷. Therefore, we anticipated that the age of our deep aquifers would play a role in the reduced availability of fixed carbon for secondary producers. However, our analysis shows no strong correlation between TOC and ⁸¹Kr age (spearman correlation coefficient = -0.11). To gain a more comprehensive understanding, it will be beneficial to compare these findings with those from more recent aquifers, as this could highlight differences in organic carbon dynamics across a wider range of aquifer ages.

Previous analyses of sulfate and carbon isotopes in the deep sandstone aquifer have suggested that bacterial sulfate reduction is a significant microbial process in the aquifer's confined zone⁴¹. Similarly, sulfate reduction is also considered a primary source of sulfide in the carbonate aquifer of the northwestern Negev⁷⁸, ~ 70 km northwest of the study area. The carbonate aquifer may receive water that is rich in organic matter from an overlying aquifer found within the Senonian chert and chalk rock formations of the Mt. Scopus Group (Fig. 1c), yielding hydrogen sulfide in the carbonate layers due to microbial oxidation of organics⁷⁸. However, in this study, we did not find prominent sulfate reducers in wells from the carbonate aquifer (C3, C4, or C5), which had high sulfide levels (48.1, 74.5, and 287.2 µmol L⁻¹, respectively). Instead, these wells were dominated by Halothiobacillales 28-57-27 chemoautotrophic sulfur oxidizers. Alternatively, organic matter might be degraded before reaching the carbonate formation⁵⁷, thereby introducing sulfidic and ammonium-rich water into the aquifer.

Another critical question concerns the source of trace oxygen, as most wells were not euxinic, and some dissolved oxygen was present at steady-state (below 6 µmol L⁻¹) (Table 1), potentially driving productivity. We consider two hypotheses: (i) a freshwater recharge component facilitated by overland flows and floods from nearby outcrops and desert streams, respectively, can introduce dissolved oxygen into the overlying carbonate aquifer; (ii) similar to other groundwater, microbial chlorite (ClO₂) dismutation could release trace oxygen levels, potentially fueling chemosynthesis⁹. We found the *cld* genes needed for chlorite reduction in 16 MAGs, including those of *Blastomonas*, *Bradyrhizobium*, *Deinococcus*, JAAYVI01 (Elusimicrobiota), and the archaeal *Nitrosotenuis*, some of which were prominent in wells S1, S2, S4, and C2 (see Supplementary Table S12, Additional File 2). This hints at dark oxygen-driven productivity in the Negev aquifers.

In addition to the pathways and processes already identified, it's crucial to consider the role of microbial communities that live attached to substrates within the aquifer matrix, which could provide a more comprehensive understanding of the microbial dynamics within these aquifers. This approach will be essential for future research to capture the full spectrum of microbial life and its functions.

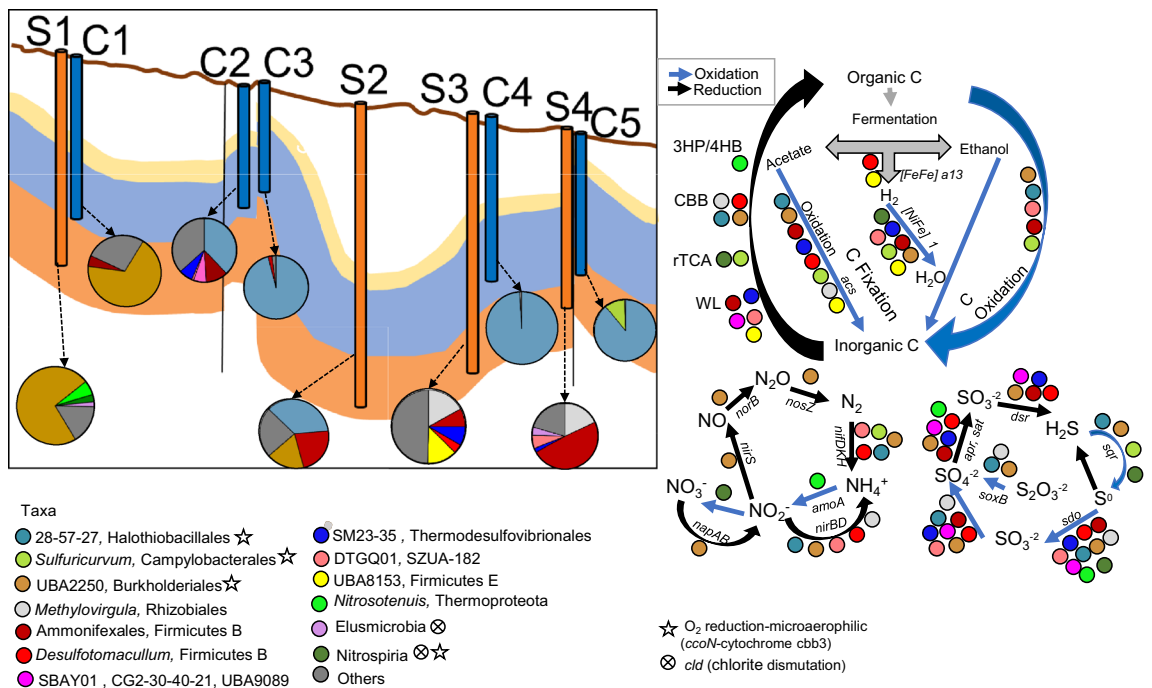


Figure 5. Metabolic reconstruction on the community scale along the eastern groundwater flow path of the two aquifers, including some of the most abundant lineages colored and grouped by their taxonomic identity. The figure summarizes biogeochemical cycling processes (carbon, nitrogen, and sulfur cycles). Each arrow indicates a single step within the cycle; genomes involved in each stage are next to each arrow; some genes encoding key enzymes are also included. The pie plots represent the relative read abundances of selected MAGs across the sampling sites. Carbon-fixation pathways: CBB—Calvin–Benson–Basham cycle, (r)TCA—(reverse) Krebs cycle. Wells from the sandstone (orange) and carbonate (blue) aquifers are shown.

Conclusions

Environmental factors are pivotal in influencing PP within aquifers¹⁴ with temperature particularly boosting productivity. This highlights that even the sandstone aquifer, known for its ancient groundwater, remains biologically active. Moreover, our findings indicate an abundance of reducing substrates and electron acceptors that could support chemosynthesis, highlighted by the diverse sulfur, hydrogen, and nitrogen transformations observed in the aquifers we studied.

Our results suggest that aquifer microbes, with a potentially versatile metabolism, can employ different strategies to efficiently harness energy and acquire carbon in these habitats, where oxygen and organic carbon are depleted (Fig. 5). The complex metabolic handoffs and other interactions in these communities are still not fully understood. Different aquifer microbiota, including eukaryotes and viruses, and their role in these systems remain to be explored. We showed that while some parameters may be shared among distinct aquifer systems (e.g. bicarbonate^{12,42}) each system has a distinct hydrogeological, lithological, mineralogical, and chemical composition, and unique biogeochemical dynamics. Higher temperatures, in particular, significantly influence microbial processes, including chemoautotrophy rates.

Data availability

The raw metagenomic reads are available at NCBI as BioProject PRJNA983765.

Received: 23 April 2024; Accepted: 29 July 2024

Published online: 05 August 2024

References

- Bar-On, Y. M., Phillips, R. & Milo, R. The biomass distribution on Earth. *Proc. Natl. Acad. Sci. USA* **115**(25), 6506–6511. <https://doi.org/10.1073/pnas.1711842115> (2018).
- Magnabosco, C. *et al.* The biomass and biodiversity of the continental subsurface. *Nat. Geosci.* **11**(10), 707–717. <https://doi.org/10.1038/s41561-018-0221-6> (2018).
- Miettinen, H. *et al.* Microbiome composition and geochemical characteristics of deep subsurface high-pressure environment Pyhäsalmi mine Finland. *Front. Microbiol.* **6**, 1203. <https://doi.org/10.3389/fmicb.2015.01203> (2015).
- Itävaara, M. *et al.* Characterization of bacterial diversity to a depth of 1500m in the Outokumpu deep borehole, Fennoscandian Shield. *FEMS Microbiol. Ecol.* **77**(2), 295–309. <https://doi.org/10.1111/j.1574-6941.2011.01111.x> (2011).
- Ragon, M., Van Diessche, A. E. S., García-Ruiz, J. M., Moreira, D. & López-García, P. Microbial diversity in the deep-subsurface hydrothermal aquifer feeding the giant gypsum crystal-bearing Naica Mine Mexico. *Front. Microbiol.* **4**, 37. <https://doi.org/10.3389/fmicb.2013.00037> (2013).

6. Kieft, T. L. *et al.* Dissolved organic matter compositions in 0.6–3.4 km deep fracture waters, Kaapvaal Craton, South Africa. *Org. Geochem.* **118**, 116–31. <https://doi.org/10.1016/j.orggeochem.2018.02.003> (2018).
7. Lau, M. C. Y. *et al.* An oligotrophic deep-subsurface community dependent on syntrophy is dominated by sulfur-driven autotrophic denitrifiers. *Proc. Natl. Acad. Sci. USA* **113**(49), E7927–E7936. <https://doi.org/10.1073/pnas.1612244113> (2016).
8. Nyssönen, M. *et al.* Taxonomically and functionally diverse microbial communities in deep crystalline rocks of the Fennoscandian shield. *ISME J.* **8**(1), 126–138. <https://doi.org/10.1038/ismej.2013.125> (2014).
9. Ruff, S. E. *et al.* Hydrogen and dark oxygen drive microbial productivity in diverse groundwater ecosystems. *Nat. Commun.* **14**, 3194. <https://doi.org/10.1038/s41467-023-38523-4> (2023).
10. Anantharaman, K. *et al.* Thousands of microbial genomes shed light on interconnected biogeochemical processes in an aquifer system. *Nat. Commun.* **7**(1), 13219. <https://doi.org/10.1038/ncomms13219> (2016).
11. Hofmann, R. & Griebler, C. DOM and bacterial growth efficiency in oligotrophic groundwater: Absence of priming and co-limitation by organic carbon and phosphorus. *Aquatic Microbial. Ecol.* **81**, 55–71. <https://doi.org/10.3354/ame01862> (2018).
12. Overholt, W. A. *et al.* Carbon fixation rates in groundwater similar to those in oligotrophic marine systems. *Nat. Geosci.* **15**, 561–567. <https://doi.org/10.1038/s41561-022-00968-5> (2022).
13. Taubert, M. *et al.* Bolstering fitness via CO₂ fixation and organic carbon uptake: mixotrophs in modern groundwater. *ISME J.* **16**(4), 1153–1162. <https://doi.org/10.1038/s41396-021-01163-x> (2022).
14. Pedersen, K. & Ekendahl, S. Assimilation of CO₂ and introduced organic compounds by bacterial communities in groundwater from southeastern Sweden deep crystalline bedrock. *Microb. Ecol.* **23**, 1–14. <https://doi.org/10.1007/BF00165903> (1992).
15. Momper, L., Jungbluth, S. P., Lee, M. D. & Amend, J. P. Energy and carbon metabolisms in a deep terrestrial subsurface fluid microbial community. *ISME J.* **11**(10), 2319–2333. <https://doi.org/10.1038/ismej.2017.94> (2017).
16. Momper, L., Casar, C. P. & Osburn, M. R. A metagenomic view of novel microbial and metabolic diversity found within the deep terrestrial biosphere at DeMMO: A microbial observatory in South Dakota, USA. *Environ. Microbiol.* **25**(12), 3719–3737. <https://doi.org/10.1111/1462-2920.16543> (2023).
17. Havig, J. R. & Hamilton, T. L. Productivity and community composition of low biomass/high silica precipitation hot springs: A possible window to earth's early biosphere?. *Life.* **9**(3), 64. <https://doi.org/10.3390/life9030064> (2019).
18. Zhou, Z., St. John, E., Anantharaman, K. & Reysenbach, A. L. Global patterns of diversity and metabolism of microbial communities in deep-sea hydrothermal vent deposits. *Microbiome.* **10**(1), 241. <https://doi.org/10.1186/s40168-022-01424-7> (2022).
19. Ram, R., Burg, A. & Adar, E. M. The Nubian Sandstone Aquifer in the Sinai Peninsula and the Negev Desert. In *Many Facet Isr Hydrogeol* (eds Kafri, U. & Yechiel, Y.) 115–41 (Springer International Publishing, Cham, 2021).
20. Ram, R. *et al.* Identifying recharge processes into a vast “fossil” aquifer based on dynamic groundwater ⁸¹Kr age evolution. *J. Hydrol.* **587**, 124946. <https://doi.org/10.1016/j.jhydrol.2020.124946> (2020).
21. Yokochi, R. *et al.* Field degassing as a new sampling method for ¹⁴C analyses in old groundwater. *Radiocarbon.* **60**(1), 349–366. <https://doi.org/10.1017/RDC.2017.64> (2018).
22. Atencio, B. *et al.* Investigating the enigma of an irregular groundwater age pattern in a confined, presumed “fossil” complex aquifer through mixing cell flow modeling. *J. Hydrol.* **630**, 130631. <https://doi.org/10.1016/j.jhydrol.2024.130631> (2024).
23. Ram, R. *et al.* Controls on the ³⁶Cl/Cl input ratio of paleo-groundwater in arid environments: New evidence from ⁸¹Kr/Kr data. *Sci. Total Environ.* **762**, 144106. <https://doi.org/10.1016/j.scitotenv.2020.144106> (2021).
24. Avrahamov, N. *et al.* Anaerobic oxidation of methane by sulfate in hypersaline groundwater of the Dead Sea aquifer. *Geobiology.* **12**(6), 511–528. <https://doi.org/10.1111/gbi.12095> (2014).
25. Yokochi, R. *et al.* Radiokrypton unveils dual moisture sources of a deep desert aquifer. *Proc. Natl. Acad. Sci.* **116**(33), 16222–16227. <https://doi.org/10.1073/pnas.1904260116> (2019).
26. Jeong, H., Park, J. & Kim, H. Determination of NH₄⁺ in environmental water with interfering substances using the modified nessler method. *J. Chem.* **2013**, 359217. <https://doi.org/10.1155/2013/359217> (2013).
27. Prjbelski, A., Antipov, D., Meleshko, D., Lapidus, A. & Korobeynikov, A. Using SPAdes De Novo Assembler. *Curr. Protoc. Bioinforma.* **70**(1), e102. <https://doi.org/10.1002/cpbi.102> (2020).
28. Kang, D. D. *et al.* MetaBAT 2: an adaptive binning algorithm for robust and efficient genome reconstruction from metagenome assemblies. *PeerJ.* **7**, 7359. <https://doi.org/10.7717/peerj.7359> (2019).
29. Wu, Y. W., Simmons, B. A. & Singer, S. W. MaxBin 2.0: An automated binning algorithm to recover genomes from multiple metagenomic datasets. *Bioinformatics.* **32**(4), 605–7. <https://doi.org/10.1093/bioinformatics/btv638> (2016).
30. Sieber, C. M. K. *et al.* Recovering of genomes from metagenomes via a dereplication, aggregation and scoring strategy. *Nat. Microbiol.* **3**, 836–843. <https://doi.org/10.1038/s41564-018-0171-1> (2018).
31. Nissen, J. N. *et al.* Improved metagenome binning and assembly using deep variational autoencoders. *Nat. Biotechnol.* **39**, 555–560. <https://doi.org/10.1038/s41587-020-00777-4> (2021).
32. Kieser, S., Brown, J., Zdobnov, E. M., Trajkovski, M. & Mccue, L. A. ATLAS: a Snakemake workflow for assembly, annotation, and genomic binning of metagenome sequence data. *BMC Bioinf.* **21**, 1–8. <https://doi.org/10.1186/s12859-020-03585-4> (2020).
33. Shaffer, M. *et al.* DRAM for distilling microbial metabolism to automate the curation of microbiome function. *Nucleic Acids Res.* **48**(16), 8883–8900. <https://doi.org/10.1093/nar/gkaa621> (2020).
34. Zhou, Z. *et al.* METABOLIC: high-throughput profiling of microbial genomes for functional traits, metabolism, biogeochemistry, and community-scale functional networks. *Microbiome.* **10**, 33. <https://doi.org/10.1186/s40168-021-01213-8> (2022).
35. Sayers, E. W. *et al.* Database resources of the national center for biotechnology information. *Nucleic Acids Res.* **50**, D20–D26. <https://doi.org/10.1093/nar/gkab1112> (2022).
36. Weissman, J. L., Hou, S. & Fuhrman, J. A. Estimating maximal microbial growth rates from cultures, metagenomes, and single cells via codon usage patterns. *Proc. Natl. Acad. Sci.* **118**(12), e2016810118. <https://doi.org/10.1073/pnas.2016810118> (2021).
37. Nielsen, E. S. Recent advances in measuring and understanding marine primary production. *J. Anim. Ecol.* **33**, 119–130. <https://doi.org/10.2307/2434> (1964).
38. Simon, M., Alldredge, A. L. & Azam, F. Bacterial carbon dynamics on marine snow. *Mar. Ecol. Prog. Ser.* **65**(3):205–11 (1990). <http://www.jstor.org/stable/24844794>
39. Geisler, E., Siebner, H., Rahav, E. & Bar-Zeev, E. Quantification of aquatic unicellular diazotrophs by immunolabeled flow cytometry. *Biogeochemistry.* **164**, 509–520. <https://doi.org/10.1007/s10533-023-01025-y> (2023).
40. R Core Team. R: A Language and Environment for Statistical Computing. 2023.
41. Vengosh, A. *et al.* New isotopic evidence for the origin of groundwater from the Nubian Sandstone Aquifer in the Negev Israel. *Appl. Geochem.* **22**(5), 1052–1073. <https://doi.org/10.1016/j.apgeochem.2007.01.005> (2007).
42. Kumar, S., Herrmann, M., Thamdrup, B. & Schwab, V. F. Nitrogen loss from pristine carbonate-rock aquifers of the hainich critical zone exploratory (Germany) is primarily driven by chemolithoautotrophic anammox processes. *Front. Microbiol.* **8**, 1951. <https://doi.org/10.3389/fmicb.2017.01951> (2017).
43. Liu, B. *et al.* Dark carbon fixation in intertidal sediments: Controlling factors and driving microorganisms. *Water Res.* **216**, 118381. <https://doi.org/10.1016/j.watres.2022.118381> (2022).
44. Zhao, Y. *et al.* Dark carbon fixation and chemolithotrophic microbial community in surface sediments of the cascade reservoirs Southwest China. *Sci. Total Environ.* **698**, 134316. <https://doi.org/10.1016/j.scitotenv.2019.134316> (2020).
45. Rosenthal, E., Zilberman, M. & Livshitz, Y. The hydrochemical evolution of brackish groundwater in central and northern Sinai (Egypt) and in the western Negev (Israel). *J. Hydrol.* **337**(3–4), 294–314. <https://doi.org/10.1016/j.jhydrol.2007.01.042> (2007).

46. Issar, A., Bein, A. & Michaeli, A. On the ancient water of the upper Nubian sandstone aquifer in Central Sinai and southern Israel. *J. Hydrol.* **17**(4), 353–374. [https://doi.org/10.1016/0022-1694\(72\)90092-3](https://doi.org/10.1016/0022-1694(72)90092-3) (1972).
47. Beaton, E. D. *et al.* Local and regional diversity reveals dispersal limitation and drift as drivers for groundwater bacterial communities from a fractured granite formation. *Front. Microbiol.* **7**, 1933. <https://doi.org/10.3389/fmicb.2016.01933> (2016).
48. Zhang, Y. *et al.* Geological activity shapes the microbiome in deep-subsurface aquifers by advection. *Proc. Natl. Acad. Sci. USA.* **119**(25), e2113985119. <https://doi.org/10.1073/pnas.2113985119> (2022).
49. Vikromvarasiri, N., Champreda, V., Boonyawanich, S. & Pisutpaisal, N. Hydrogen sulfide removal from biogas by biotrickling filter inoculated with *Halothiobacillus neapolitanus*. *Int. J. Hydrogen Energy.* **42**(29), 18425–18433. <https://doi.org/10.1016/j.ijhydene.2017.05.020> (2017).
50. Kojima, H., Watanabe, M., Miyata, N. & Fukui, M. Sulfuricystis multivorans gen. nov., sp. nov. and Sulfuricystis thermophila sp. nov., facultatively autotrophic sulfur-oxidizing bacteria isolated from a hot spring, and emended description of the genus Rugosibacter. *Arch. Microbiol.* **204**(9), 595. <https://doi.org/10.1007/s00203-022-03186-0> (2022).
51. Sauder, L.A., Engel, K., Lo, C., Chain, P. & Neufeld, J.D. *Candidatus Nitrosotenuis aquarius*, an Ammonia-Oxidizing Archaeon from a Freshwater Aquarium Biofilter. Löffler FE, editor. *Appl. Environ. Microbiol.* **84**(19), e01430–18 (2018). <https://doi.org/10.1128/AEM.01430-18>
52. Fowler, S. J., Palomo, A., Dechesne, A., Mines, P. D. & Smets, B. F. Comammox *Nitrospira* are abundant ammonia oxidizers in diverse groundwater-fed rapid sand filter communities. *Environ. Microbiol.* **20**(3), 1002–1015. <https://doi.org/10.1111/1462-2920.14033> (2018).
53. Robinson, J. J. *et al.* Kinetic isotope effect and characterization of form II RubisCO from the chemoautotrophic endosymbionts of the hydrothermal vent tubeworm *Riftia pachyptila*. *Limnol. Oceanogr.* **48**(1), 48–54. <https://doi.org/10.4319/lo.2003.48.1.00048> (2003).
54. Berg, I. A. Ecological aspects of the distribution of different autotrophic CO₂ fixation pathways. *Appl. Environ. Microbiol.* **77**(6), 1925–1936. <https://doi.org/10.1128/AEM.02473-10> (2011).
55. Alves, J.I., *et al.* Effect of Sulfate on carbon monoxide conversion by a thermophilic syngas-fermenting culture dominated by a *Desulfovifundulus* Species. *Front. Microbiol.* **11**, 588468. (2020) <https://doi.org/10.3389/fmicb.2020.588468>
56. Fang, Y. *et al.* Compositional and metabolic responses of autotrophic microbial community to salinity in lacustrine environments. *Msystems.* **7**(4), e00335-e422. <https://doi.org/10.1128/msystems.00335-22> (2022).
57. Burg, A., Zilberbrand, M. & Yechiel, Y. Radiocarbon variability in groundwater in an extremely arid zone—the arava valley Israel. *Radiocarbon.* **55**(2), 963–978. <https://doi.org/10.1017/S0033822200058112> (2013).
58. Magnabosco, C. *et al.* A metagenomic window into carbon metabolism at 3 km depth in Precambrian continental crust. *ISME J.* **10**(3), 730–741. <https://doi.org/10.1038/ismej.2015.150> (2016).
59. Wu, X. *et al.* Microbial metagenomes from three aquifers in the Fennoscandian shield terrestrial deep biosphere reveal metabolic partitioning among populations. *ISME J.* **10**, 1192–1203. <https://doi.org/10.1038/ismej.2015.185> (2016).
60. Grimm, F., Franz, B. & Dahl, C. Thiosulfate and Sulfur Oxidation in Purple Sulfur Bacteria. In: *Microbial Sulfur Metabolism*. Berlin, Heidelberg: Springer Berlin Heidelberg, 101–16. (2008) https://doi.org/10.1007/978-3-540-72682-1_9
61. Ghosh, W. & Dam, B. Biochemistry and molecular biology of lithotrophic sulfur oxidation by taxonomically and ecologically diverse bacteria and archaea. *FEMS Microbiol. Rev.* **33**(6), 999–1043. <https://doi.org/10.1111/j.1574-6976.2009.00187.x> (2009).
62. Lin, L.-H., Slater, G.E., Sherwood Lollar, B., Lacrampe-Coulocum, G. & Onstott, T.C. The yield and isotopic composition of radiolytic H₂, a potential energy source for the deep subsurface biosphere. *Geochim. Cosmochim. Acta.* **69**(4):893–903 (2005). <https://doi.org/10.1016/j.gca.2004.07.032>
63. Mazor, E. Radon and radium content of some Israeli water sources and a hypothesis on underground reservoirs of brines, oils and gases in the Rift Valley. *Geochim. Cosmochim. Acta.* **26**, 765–786 (1962).
64. Minster, T., Ilani, S., Kronfeld, J., Even, O. & Godfrey-Smith, D. I. Radium contamination in the Nizzana-1 water well, Negev Desert, Israel. *J. Environ. Radioact.* **71**(3), 261–273. [https://doi.org/10.1016/S0265-931X\(03\)00173-5](https://doi.org/10.1016/S0265-931X(03)00173-5) (2004).
65. Dzaugis, M. E., Spivack, A. J., Dunlea, A. G., Murray, R. W. & D'Holdt, S. Radiolytic hydrogen production in the subseafloor basaltic aquifer. *Front. Microbiol.* **7**, 76. <https://doi.org/10.3389/fmicb.2016.00076> (2016).
66. Kumar, S., *et al.* Thiosulfate- and hydrogen-driven autotrophic denitrification by a microbial consortium enriched from groundwater of an oligotrophic limestone aquifer. *FEMS Microbiol. Ecol.* **94**(10), fyy141 (2018). <https://doi.org/10.1093/femsec/fyy141>
67. Henson, W. R., Huang, L., Graham, W. D. & Ogram, A. Nitrate reduction mechanisms and rates in an unconfined eogenetic karst aquifer in two sites with different redox potential. *J. Geophys. Res.: Biogeosci.* <https://doi.org/10.1002/2016JG003463> (2017).
68. Mosley, O. E. *et al.* Nitrogen cycling and microbial cooperation in the terrestrial subsurface. *ISME J.* **16**(11), 2561–2573. <https://doi.org/10.1038/s41396-022-01300-0> (2022).
69. Swanner, E.D. & Templeton, A.S. Potential for nitrogen fixation and nitrification in the granite-hosted subsurface at Henderson Mine, CO. *Front. Microbiol.* **2**, 254. (2011) <https://doi.org/10.3389/fmicb.2011.00254>
70. Rubin-Blum, M. *et al.* Active microbial communities facilitate carbon turnover in brine pools found in the deep Southeastern Mediterranean Sea. *Mar. Environ. Res.* **198**, 106497. <https://doi.org/10.1016/j.marenres.2024.106497> (2024).
71. Kirchman, D. L., Morán, X. A. G. & Ducklow, H. Microbial growth in the polar oceans - Role of temperature and potential impact of climate change. *Nat. Rev. Microbiol.* **7**(6), 451–459. <https://doi.org/10.1038/nrmicro2115> (2009).
72. McDonough, L. K. *et al.* Changes in global groundwater organic carbon driven by climate change and urbanization. *Nat. Commun.* **11**(1), 1279. <https://doi.org/10.1038/s41467-020-14946-1> (2020).
73. Ram, R. *et al.* Large-scale paleo water-table rise in a deep desert aquifer recorded by dissolved noble gases. *J. Hydrol.* **612**, 128114. <https://doi.org/10.1016/j.jhydrol.2022.128114> (2022).
74. Hillel, D. Introduction to Environmental Soil Physics. *Acad. Press.* 2004.
75. Nativ, R., Bachmat, Y. & Issar, A. Potential use of the deep aquifers in the Negev Desert, Israel—a conceptual model. *J. Hydrol.* **94**, 237–265. [https://doi.org/10.1016/0022-1694\(87\)90055-2](https://doi.org/10.1016/0022-1694(87)90055-2) (1987).
76. Calvo, R. & Gvirtzman, Z. Assessment of CO₂ storage capacity in southern Israel. *Int. J. Greenh. Gas Control.* **14**, 25–38. <https://doi.org/10.1016/j.ijggc.2012.12.027> (2013).
77. McDonough, L.K. *et al.* A new conceptual framework for the transformation of groundwater dissolved organic matter. *Nat Commun.* **13** 2153. <https://doi.org/10.1038/s41467-022-29711-9> (2022).
78. Burg, A., Gavrieli, I. & Guttmann, J. Concurrent salinization and development of anoxic conditions in a confined aquifer, southern Israel. *Groundwater.* **55**(2), 183–198. <https://doi.org/10.1111/gwat.12474> (2017).

Acknowledgements

The authors thank the Israel Water Authority and Mekorot Israel National Water Company for providing access to wells for sampling and sharing data. Special thanks are extended to Oded Beja, Alina Pushkarev, and Ariel Chazan (Technion – Israel Institute of Technology) for their assistance with the field sampling method. We also thank Damiana Diaz Reck, Almog Gafni, Adva Speter, Amos Russak, and Efrat Eliani Russak (Ben-Gurion University of the Negev) for their precise analytical work and technical assistance, and Alexandra Gonzalez (Technological University of Panama) for her assistance in preparing the location map.

Author contributions

The study was conceived and funded by MR-B, EMA, and ZR. BA, EMA, RR, and ZR collected the samples with the help of EG and MR-B, and EG and EB-Z performed the productivity measurements. MR-B performed the bioinformatics work. BA, MR-B, and ZR wrote the paper with contributions from all co-authors. The final manuscript was read and approved by all authors.

Funding

This work was funded by the Israel Science Foundation (Grant number: 1068/20). MR-B is funded by the Ministry of Energy (Grant 221-17-002), a Ministry of Science and Technology grant (Proposal #001126), and the Israeli Science Foundation (ISF) grant 1359/23. The research was also supported by grants from the National Secretariat of Science, Technology, and Innovation (SENACYT) of the Republic of Panama to BA.

Competing interests

The authors declare no competing interests.

Additional information

Supplementary Information The online version contains supplementary material available at <https://doi.org/10.1038/s41598-024-68868-9>.

Correspondence and requests for materials should be addressed to Z.R.

Reprints and permissions information is available at www.nature.com/reprints.

Publisher's note Springer Nature remains neutral with regard to jurisdictional claims in published maps and institutional affiliations.

Open Access This article is licensed under a Creative Commons Attribution-NonCommercial-NoDerivatives 4.0 International License, which permits any non-commercial use, sharing, distribution and reproduction in any medium or format, as long as you give appropriate credit to the original author(s) and the source, provide a link to the Creative Commons licence, and indicate if you modified the licensed material. You do not have permission under this licence to share adapted material derived from this article or parts of it. The images or other third party material in this article are included in the article's Creative Commons licence, unless indicated otherwise in a credit line to the material. If material is not included in the article's Creative Commons licence and your intended use is not permitted by statutory regulation or exceeds the permitted use, you will need to obtain permission directly from the copyright holder. To view a copy of this licence, visit <http://creativecommons.org/licenses/by-nc-nd/4.0/>.

© The Author(s) 2024